CHEMISTRY OF MATERIALS

ARTICLE

pubs.acs.org/cm

Cascade Organic Solar Cells

Cody W. Schlenker,[†] Vincent S. Barlier,[†] Stephanie W. Chin,[‡] Matthew T. Whited,[†] R. Eric McAnally,[†] Stephen R. Forrest,[§] and Mark E. Thompson*[,†,‡]

[†]Department of Chemistry and Center for Energy Nanoscience, University of Southern California, Los Angeles, California 90089, United States

[‡]Viterbi School of Engineering, University of Southern California, Los Angeles, California 90089, United States

[§]Department of Electrical Engineering and Computer Science and Department of Physics, University of Michigan, Ann Arbor, Michigan 48109, United States

Supporting Information

ABSTRACT: We demonstrate planar organic solar cells consisting of a series of complementary donor materials with cascading exciton energies, incorporated in the following structure: glass/indium-tin-oxide/donor cascade/C_{60}/bathocuproine/Al. Using a tetracene layer grown in a descending energy cascade on 5,6-diphenyl-tetracene and capped with 5,6,11,12-tetraphenyl-tetracene, where the accessibility of the π-system in each material is expected to influence the rate of parasitic carrier leakage and charge recombination at the donor/acceptor interface, we observe an increase in open circuit voltage (V_{oc}) of approximately 40% (corresponding to a change of +200 mV) compared to that of a single tetracene donor. Little change is observed in other parameters such as fill factor and short circuit current density ($FF = 0.50 \pm 0.02$ and $J_{sc} = 2.55 \pm 0.23$ mA/cm^2) compared to those of the control tetracene−C_{60} solar cells ($FF = 0.54 \pm 0.02$ and $J_{sc} = 2.86 \pm 0.23$ mA/cm^2). We demonstrate that this cascade architecture is effective in reducing losses due to polaron pair recombination at donor−acceptor interfaces, while enhancing spectral coverage, resulting in a substantial increase in the power conversion efficiency for cascade organic photovoltaic cells compared to tetracene and pentacene based devices with a single donor layer.

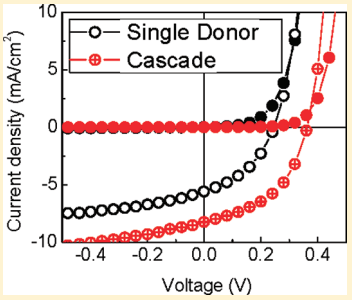

KEYWORDS: organic solar cells, photovoltaics, excitation transfer, energy cascade, open circuit voltage, polaron pair, charge transfer state

INTRODUCTION

As a result of the use of low-cost materials, ease of processing, and recent increases in power conversion efficiencies,[1] organic photovoltaic (OPV) cells have attracted considerable attention as a potentially practical approach to solar energy harvesting.[2] Although organics have found uses in light emitting diodes[3] and organic thin film transistors[4] and sensors,[5] the current OPV performance (including efficiency, reliability, and a demonstrated low cost path to manufacture) falls short of that required to make this technology attractive for widespread deployment. One promising avenue for improving their power conversion efficiency (η_p) is to increase the short circuit current density (J_{sc}) by harvesting photons across the solar spectrum. However, maximizing the electrical output power density (P_{max}), resulting in high η_p, requires balance among materials properties to also achieve high open circuit voltage (V_{oc}) and fill factor ($FF = P_{max}/J_{sc}V_{oc}$). Here, we demonstrate an energy cascade architecture that distributes materials requirements among several complementary absorbing layers. This approach allows the control of interfacial electronic coupling to maximize V_{oc}, while enhancing spectral coverage for increased short circuit current. While cascade device architectures have been previously considered for spatially directing excitation, the potential for such architectures to relax material design rules, which are otherwise difficult to fulfill using conventional single-donor architectures, goes beyond the previous reports of cascade architectures that focused primarily on improving energy transfer across the donor region of an OPV.[6]

The Cascade Concept. Optical-to-electrical energy conversion in OPVs occurs as a result of photoinduced electron transfer between an excited molecular electron-donor (D) and an electron-accepting molecule (A). Alternatively, electron transfer between D and an excited A is also possible. Photon absorption leads to a localized excited state (exciton) that diffuses to the donor/acceptor interface. Charge transfer quenching of the exciton at the D/A interface produces a Coulombically bound polaron pair or charge transfer (CT) state, represented as D^+A^-. The separation of charge from the CT state produces free holes and electrons that are collected at the anode and cathode, respectively. Ultimately, J_{sc}, V_{oc}, FF, and η_p are determined by the thermodynamics and kinetics of several processes. Separate optimization of these processes is the motivation for the cascade architecture.

Received: February 18, 2011
Revised: August 5, 2011
Published: September 02, 2011

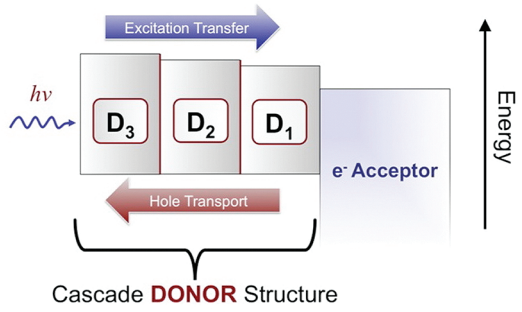

Figure 1. Schematic of the photoactive region for an example cascade architecture in which the donor layer comprises three complementary materials: D_1, D_2, and D_3.

Often, properties of a specific donor material that favorably impact one performance metric negatively impact another. For example, molecular geometries that frustrate intermolecular electronic interactions have been implicated in increasing V_{oc};[7] however, exciton diffusion and charge transport are generally enhanced by strong interactions in these materials.[8] This competition makes it difficult to identify a single donor or acceptor material that fulfills these conflicting requirements. As an alternative, consider the architecture in Figure 1, where the donor region of the device is partitioned into a multilayer stack of complementary materials, D_1, D_2, and D_3, with thin layers of D_1 and D_3 as "bookends" to the principal donor layer, D_2. Here, D_3 is designed to prevent exciton diffusion to the anode and suppress dark current, while D_1 is chosen to facilitate exciton transfer to the D/A interface while leading to an increased V_{oc}. In this work, we demonstrate such an architecture that distributes materials requirements among several absorbing layers whose frontier orbital energies promote exciton diffusion toward the donor−acceptor junction. This results in a high V_{oc} while improving the solar spectral coverage to yield a high short circuit current.

EXPERIMENTAL METHODS

Materials. Tetracene (Aldrich; 98%), rubrene (Aldrich; powder), pentacene (Aldrich; 93.5%), aluminum phthalocyanine chloride (Aldrich; 85%), C_{60} (MER; 99+%), and bathocuproine (Aldrich; 96%) were obtained from commercial sources and purified via thermal gradient sublimation (~0.2 μTorr). Aluminum (Alfa Aesar; 99.999%) and molybdenum trioxide (Aldrich; 99.5%) were obtained from commercial sources and used as received. 5,6-Diphenyl-tetracene (Dpt) and 5,6-dinaphthyl-tetracene (Dnt) were prepared as reported elsewhere.[9] Glass substrates commercially coated with ITO (thickness, 1500 ± 100 Å; sheet resistance, 20 ± 5 Ω/cm^2; transmission, 84% at 550 nm) were purchased from Thin Film Devices Inc.

Film Growth and Characterization. Device substrates were solvent-cleaned and placed in an ozone atmosphere (UVOCS T10X10/OES) for 10 min immediately before they were loaded into the high vacuum (~2 μTorr) deposition chamber. Layer thickness and deposition rates were monitored by a quartz crystal microbalance (Inficon) calibrated using monochromatic (Rudolph Technologies, Inc.; Auto EL) or spectroscopic (J. A. Woollam Co., Inc.; WVASE32) ellipsometry. Films of Dpt, rubrene (Rbn), and aluminum phthalocyanine chloride (ClAlPc) were grown by thermal evaporation at a rate from 0.5 to 1.0 Å/s, and tetracene (Ttn) and pentacene (Ptn) films were grown at the rates 18.0−20.0 and 8.0−15.0 Å/s, respectively. A growth rate of 2 Å/s was used for MoO_3, C_{60}, BCP, and Al. Unless otherwise specified, 1000 Å thick Al cathodes were used. Condensed phase optical measurements were performed on solvent-cleaned glass, quartz, or polished silicon substrates using an Agilent 8453 spectrophotometer and Photon Technology International fluorimeter. Thin film transflectance measurements were performed on multilayer samples in a Perkin-Elmer Lambda 950 UV/vis/NIR spectrophotometer with a 150 mm diameter integrating sphere, using Al-coated glass as a reference. Atomic force microscopy (AFM) was performed using a Digital Instruments Nanoscope Dimension 3100 atomic force microscope. Grazing incidence X-ray diffraction measurements were performed on a Rigaku Ultima IV diffractometer using a Cu Kα radiation source (λ = 1.54 Å).

Device Characterization. Current−voltage measurements were performed at ambient temperature using a Keithly 2420 SourceMeter in the dark and under corrected 1 kW m^{-2} white light illumination from a 300 W xenon arc lamp (Newport Oriel Product Line) equipped with an AM 1.5G filter. Spectral mismatch correction was performed as described in the literature[10] using a silicon photodiode (Hamamatsu S1787-04, 8RA filtered or S1787-12, KG5 filtered) calibrated at the National Renewable Energy Laboratory (NREL) and frequency modulated illumination (250 Hz) from a Xe source coupled to a Cornerstone 260 $^1/_4$m monochromator (Newport 74125) in conjunction with an EG&G 7220 DSP Lock-In amplifier. This monochromatic system was also used to collect all external quantum efficiency data.

RESULTS AND DISCUSSION

Charge Recombination and Open Circuit Voltage. Charge recombination at the donor/acceptor (D/A) interface is a principal source of the dark current that limits V_{oc}.[1a,11] This reaction between positive (at D^+) and negative (at A^-) polarons bound at the interface D^+A^- occurs at a rate which can be described by the Marcus theory for outer sphere electron transfer. As previously determined, the rate constant for recombination (k_{rec}) can be obtained from the current density (J) vs voltage characteristics in the dark, given by[12]

$$J = J_s\left\{\exp\left(q\frac{V - JR_s}{nkT}\right) - 1\right\} + \frac{V - JR_s}{R_p} - J_{ph} \qquad (1)$$

where R_s and R_p represent all series and parallel specific resistances that often serve as proxies for a range of charge transport and recombination processes.[11b] Also, J_{ph} is the photocurrent density, n is the ideality factor, and J_s is the saturation current density. Because eq 1 can be rewritten at open circuit (J = 0) to give eq 2,

$$V_{oc} = \frac{nkT}{q}\ln\left\{\frac{J_{sc}}{J_s} + 1 - \frac{V_{oc}}{J_sR_p}\right\} \approx \frac{nkT}{q}\ln\left\{\frac{J_{sc}}{J_s}\right\} \qquad (2)$$

where we assume $R_p \rightarrow \infty$, $R_s \rightarrow 0$, and $J_{ph} \gg J_s$, we conclude that minimizing k_{rec} will decrease J_s, maximizing V_{oc}, as previously observed.[1a,7,11a,11b,13] In the recombination-limited forward bias regime (where $n \approx 2$),[11a,b,14] polaron dynamics influence the maximum value of V_{oc} in organic solar cells. These dynamic parameters include the rate of free polaron reaction with trapped polarons of opposite charge at the D/A interface to form polaron pairs (or charge transfer complexes, D^+A^-),[11a,b] the reaction order for charge carrier recombination,[15] and the rate of polaron pair recombination. Significant attention has also been given to determining macroscopic rate laws for bimolecular charge recombination, with the results suggesting that such kinetics influence both V_{oc} and FF.[15,16] Recently, interest in defining molecular properties that give rise to the voltage losses

Scheme 1. Chemical Structures for Tetracene (Ttn), 5,6-Diphenyl-tetracene (Dpt), Rubrene (Rbn), and 5,6-Dinaphthyl-tetracene (Dnt)

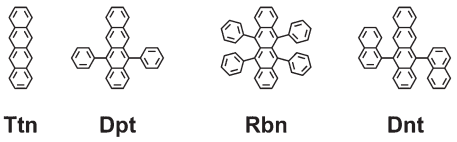

subsumed under J_s in eq 2 has increased.[7b,11a,17] The saturation current density has been previously expressed as[11b]

$$J_s = qa_0\left(\frac{k_{rec,CT}}{k_{d,CT} + k_{rec,CT}}\right)2k_f NH \exp\left(\frac{-\Delta E_{HL}}{n_{sym}kT}\right) \quad (3)$$

where the rate constant is $k_{rec,CT}$ for CT-to-neutral state recombination for a symmetric device with identical electron and hole transport properties and trap distributions. Here, the volume occupied by the CT complex is $(4/3\pi)\ a_0^3$, k_f is the rate constant for the reaction of free polarons with oppositely charged polarons trapped at the D/A interface to form D^+A^-, N is the density of states for the donor HOMO or the acceptor LUMO, H is the total trap density, and $k_{d,CT}$ is the rate constant for the dissociation of D^+A^- to yield free polarons. As previously described,[11b] n_{sym} is the ideality factor for the symmetric device. The quantity ΔE_{HL} is the energy difference between the highest occupied molecular orbital (HOMO) of the donor and the lowest unoccupied molecular orbital (LUMO) of the acceptor, along with any shift due to formation of an interface dipole.[1a,24] Note that k_f is determined by the dielectric constant and charge mobility in the organic layers. All else being equal, from eqs 2 and 3, it follows that suppression of J_s by limiting $k_{rec,CT}$ will maximize V_{oc}.

While radiative contributions to J_s, such as charge transfer state emission,[18] have been observed for organic solar cells, nonradiative contributions to J_s have been identified as a significant source of voltage loss.[13] Hence, one route to maximize V_{oc} is to limit the nonradiative decay rate of D^+A^- at the D/A interface.[11b] The nonradiative contribution to $k_{rec,CT}$ is given by the Marcus theory, as follows:

$$k_{rec,CT}^{NR} = \frac{4\pi^2}{h}H_{ij}^2\frac{1}{\sqrt{4\pi\lambda kT}}\exp\left\{\frac{-(\Delta G^\circ + \lambda)^2}{4\lambda kT}\right\} \quad (4)$$

where h is Planck's constant, H_{ij} is the electronic coupling matrix element between the initial charge transfer state (j) and the final neutral state (i), λ is the reorganization energy, and ΔG° is the total change in free energy. For $\Delta G^\circ > \lambda$, nonradiative recombination occurs in the Marcus inverted regime, with $k_{rec,CT}^{NR}$ decreasing exponentially with the square of ΔG°.

The V_{oc} has been shown to be proportional to the energy difference, ΔE_{HL}. In this context, $\Delta E_{HL} \approx \Delta G^\circ$. Hence, an increase in ΔE_{HL} decreases $k_{rec,CT}^{NR}$ and J_s, thereby leading to an increase in V_{oc}. Here, we explore the alternative route to decreasing $k_{rec,CT}^{NR}$ and J_s by decreasing electronic coupling at the D/A interface, that is, by decreasing H_{ij} rather than increasing ΔE_{HL}.

Decreasing H_{ij} has been suggested as a route to increasing V_{oc}.[7,13,19] We have shown that increasing the separation between the donor and acceptor by adding steric bulk to the donor[7b] or acceptor[17] moieties can result in an increase in V_{oc}. Increasing the D/A molecular separation leads to a decrease in the electronic interaction between the donor and acceptor and, thus, a decrease in H_{ij}. Unfortunately, adding steric bulk to a molecular species can have unintended side effects, because the bulkier molecule will have a lower molecular density and will give lower absorption coefficients. The added steric bulk may also lead to reduced exciton diffusion lengths and charge carrier mobilities. For example, the open circuit voltage was observed to correlate with increasing π-system shielding for the series (chemical structures shown in Scheme 1) tetracene (Ttn, V_{oc} = 0.55 V) < 5,6-diphenyl-tetracene (Dpt, V_{oc} = 0.65 V) < rubrene (Rbn, V_{oc} = 0.92 V) < 5,6-dinaphthyl-tetracene (Dnt, V_{oc} = 1.06 V) in acene/C_{60} based devices,[7b,9] despite their similar HOMO energies.[9,20] The observed V_{oc} enhancement is a result of a reduced H_{ij} as a result of steric shielding by the aryl substituents.[7b] However, while Ttn forms dense polycrystalline thin films with a high absorption coefficient and related exciton and charge transport properties,[21] the other three materials form amorphous films, resulting in low device fill factor and photocurrent for the ITO/acene/C_{60}/BCP/Al OPVs.[9] We show below that the cascade donor architecture is effective in balancing these potentially contradictory requirements.

Identifying and Characterizing Cascade Donor Structures. Donor materials for cascade structures were considered on the basis of the energy ordering of the excitonic states (E_{00}) for materials D_1–D_3 ($D_3 > D_2 > D_1$) to form an excitation transfer pathway to the D/A interface. This is illustrated in Figure 2a for the series Dpt, Ttn, and Rbn, where the intersection of the thin-film excitation and emission spectra gives E_{00} for these fluorescent materials. We note that evidence exists in support of the presence of thermally activated singlet exciton fission in Ttn films,[22] making this material an interesting candidate for high efficiency solar cells,[23] as previously suggested.[24] The orthogonally oriented phenyl rings of Dpt and Rbn couple slightly to the tetracene core, red shifting the solution absorption compared to that of Ttn by λ = 10 and 30 nm, respectively. However, while molecular aggregation significantly red shifts the thin film Ttn absorption, the neat Dpt and Rbn spectra are relatively unperturbed. As a result, the S_1 exciton energies for this series are consistent with the cascade criterion, as shown in Figure 2a. Excitation in Dpt may Förster transfer to Ttn and, likewise, Ttn excitations to Rbn. We note that interfacial excitation transfer between chromophores via electron exchange (Dexter mechanism) may also occur and that Ttn[22b] and Rbn[25] possess similar lowest triplet excited state energies of 1.3 eV. Thus, we anticipate no blocking of triplet excitons produced via activated singlet fission in the Ttn layer at the Ttn/Rbn interface.

To ensure monopolar charge transport, the ionization energy (E_i^*) for $D^* \rightarrow D^+ + e^-$ of, for example, D_3 relative to the electron affinity of material D_2, must lead to endergonic exciton dissociation at the D_3/D_2 interface. This criterion is also met by the Dpt/Ttn/Rbn system as depicted in Figure 2b. Barriers to hole injection from D_1 to D_2 and from D_2 to D_3 must be minimized to preclude charge trapping. As in Figure 2b, hole injection from Rbn (E_i = −5.3 eV)[26] to Ttn (E_i = −5.3 eV)[20a,27] is thermoneutral and is only slightly endothermic from Ttn to Dpt (E_i = −5.4 eV).[28] Thus, the cascade structure Dpt/Ttn/Rbn, where D_3 = Dpt, D_2 = Ttn, and D_1 = Rbn, meets the excitation transfer requirements while introducing a minimal barrier to charge extraction.

The thin film excitation and emission spectra for Ttn, Dpt, and Rbn in Figure 2a exhibit significant spectral overlap. To determine

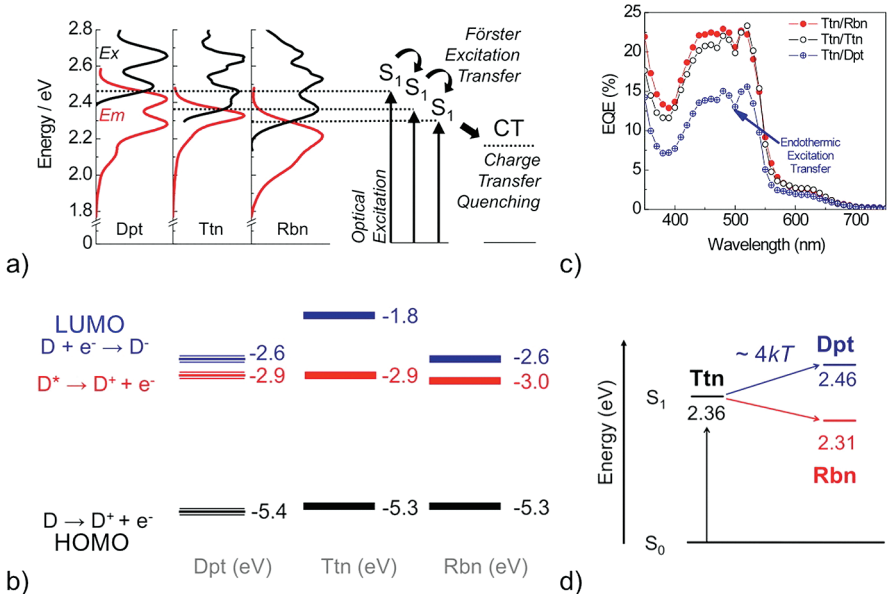

Figure 2. (a) Cascading exciton energies for the series diphenyltetracene (Dpt), tetracene (Ttn), and rubrene (Rbn) shown by neat film excitation (Ex) and emission (Em) spectra. While this mechanism suggests Förster-assisted excitation transfer of singlet excitons, note that electron exchange (Dexter type) and the transfer of triplet excitation may also lead to the population of the charge transfer (CT) state at the charge donor/acceptor interface. (b) Thin film ionization energies (black), excited state ionization energies (red), and electron affinities (blue) for Dpt, Ttn, and Rbn. Broken lines represent values estimated from solution electrochemical data as previously reported.[32] Solid lines represent values measured or derived from ultraviolet photoelectron spectroscopy[20a,27b−27d] or inverse photoemission spectroscopy data.[26a,33] (c) External quantum efficiency for photovoltaic devices consisting of ITO/donor/C_{60} (400 Å)/BCP (100 Å)/Al, where the donor is a 650 Å thick Ttn film coated with an additional 50 Å of either Rbn (red circle), Dpt (blue circle cross), or Ttn (open circle). (d) Optical excitation energies derived from part a, suggesting excitation transfer from Ttn to Dpt, will be endothermic by ~$4kT$, while excitation transfer from tetracene to rubrene will be slightly exothermic, resulting in the EQE shown in part c.

the excitation transfer efficiency through the interfacial layer, we measured the external quantum efficiency (EQE) for devices in which absorption occurs primarily in a thick layer of tetracene, followed by insertion of a thin interfacial layer of either Dpt, Ttn, or Rbn. The EQE data for C_{60}-acceptor-based OPVs with 650 Å thick nanocrystalline tetracene donor films coated with 50 Å of Ttn, Dpt, or Rbn (i.e., ITO/Ttn (650 Å)/acene (50 Å)/C_{60}/BCP/Al) are shown in Figure 2c. These devices derive their primary acene absorption from the thick Ttn layer, ensuring consistent Ttn film morphology in all three devices because all three devices have Ttn layers deposited directly on ITO. Thus, we expect that the exciton diffusion length in the bulk of the donor layer (i.e., Ttn) is unchanged for the three devices. Differences in EQE for the OPVs with a 50 Å Ttn, Dpt, or Rbn layer are, therefore, primarily as a result of differences in exciton transfer efficiency at the Ttn/acene interface. The Ttn- and Rbn-capped devices yield nearly identical EQE responses. However, the Dpt-capped device exhibits a 30% reduction in EQE. Excitation transfer from Ttn to Dpt is slightly endothermic, as shown in Figure 2d. Thus, the Dpt layer reduces the migration efficiency of excitons from Ttn to the D/A interface, leading to a small loss in EQE for Ttn/Dpt, while excitation transfer in Ttn/Rbn does not reduce EQE. These data suggest that efficient excitation transfer will also occur in the excitation-cascade system according to Figure 1, where D_1 = Rbn, D_2 = Ttn, and D_3 = Dpt.

The performances of cascade solar cells consisting of ITO/Dpt (x)/Ttn (y)/Rbn (z)/C_{60} (400 Å)/BCP (100 Å)/Al, $x + y + z$ = 450 Å, were compared to those of a tetracene-based single donor device (y = 450 Å, x, z = 0, device A). Several OPVs have been reported with Ttn donor and C_{60} acceptor layers, with power efficiencies ranging η_P = 0.6−2.3%.[7b,21a,24,29] The variability in the efficiencies reported is due to the variation of a number of parameters, including materials purity, device architecture, deposition conditions for the organic and electrode materials, and OPV testing conditions such as light intensity and temperature. All of the devices reported here were prepared using high purity multiply sublimed materials and identical deposition conditions, and they were tested under 1 sun illumination corrected for spectral mismatch[10] using a filtered silicon photodiode calibrated at the National Energy Renewable Laboratory (NREL) to give efficiencies at AM1.5G spectral irradiance, as described in the Experimental Methods. The data are for a single typical device taken from a population fabricated in a single fabrication run. In Figure 3a the $J-V$ characteristics for device B with x = 50 Å, y = 200 Å, z = 200 Å are compared to those of device A in the dark and under AM 1.5G 1 sun (1 kW/m^2) illumination. For device A, we obtain V_{oc} = 0.54 ± 0.01 V, J_{sc} = 2.86 ± 0.23 mA/cm^2, and FF = 0.54 ± 0.02. However, for device B (see Table 1), we see a 200 mV enhancement in photovoltage, resulting in V_{oc} = 0.74 ± 0.01 V, with J_{sc} = 2.55 ± 0.23 mA/cm^2 and FF = 0.50 ± 0.02, comparable to those of device A.

The small discrepancy in J_{sc} between devices A and B is attributed to two factors: (i) a reduced exciton diffusion length for Ttn grown on Dpt rather than directly on the ITO in device A (on the basis of X-ray diffraction studies, *vide infra*) and (ii) lower absorption coefficients for the Dpt and Rbn layers relative to Ttn (see the Supporting Information). This is supported by device C, where the donor layer is composed of 100 Å Dpt and 350 Å Ttn. This device gives a markedly lower J_{sc} than device A, as expected for both factors i and ii. The FF of device C is also lower than that of either device A or B, consistent with the reduced hole

dx.doi.org/10.1021/cm200525h |*Chem. Mater.* 2011, 23, 4132–4140

conductivity for Dpt. In addition, singlet exciton fission in the Dpt layer, for which the T_1 state is slightly lower in energy than the T_1 state of Ttn,[31] may lower the quantum yield for excitation transfer from Dpt to Ttn. These observations are also consistent with the data showing that device B (V_{oc} = 0.74 ± 0.01 V) does not completely recover the photovoltage produced in single-donor Rbn devices (V_{oc} = 0.92 V) with the structure ITO/Rbn (200 Å)/C_{60} (400 Å)/BCP (Å)/Al (see Table 1.) Moreover, although the Rbn and Dpt/Ttn/Rbn devices produce comparable photocurrents, J_{sc} = 2.4 ± 0.2 and 2.6 ± 0.2 mA/cm^2, respectively, the *FF* for the Rbn device is only 0.43, which is lower than that of either device A or B, which incorporate crystalline Ttn layers.

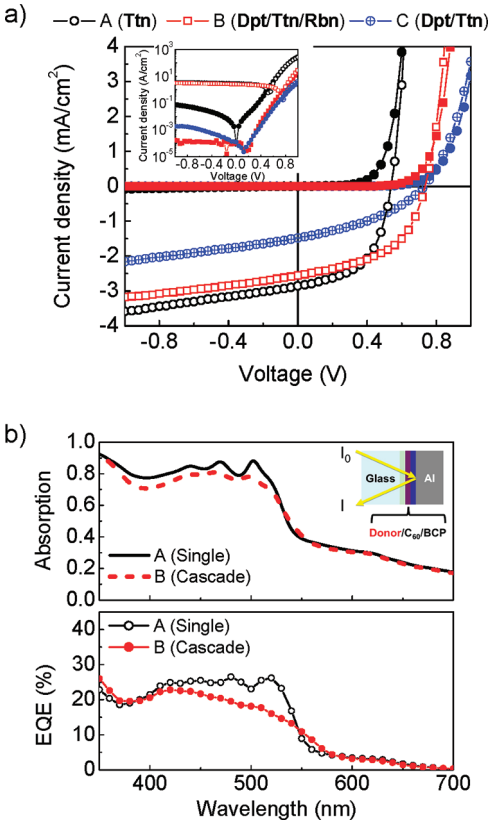

Figure 3. (a) Electrical characteristics for the tetracene-based cascade devices B (red open square) and C (blue circle cross), relative to device A with only a single tetracene donor (open circle). Characteristics recorded under 1 sun AM1.5G illumination are shown as open symbols, and those recorded in the dark are shown as closed symbols. Devices B and C give roughly 200 mV higher V_{oc} than device A. Devices consist of ITO/Donor (450 Å)/C_{60} (400 Å)/BCP (100 Å)/Al, where Donor is either a single layer of neat Ttn (device A) or Dpt (50 Å)/Ttn (200 Å)/Rbn (200 Å) (device B) or Dpt (100 Å)/Ttn (350 Å) (device C). Inset: Semilog plot of the current−voltage characteristics. (b) Spectral absorption for organic layers in devices A and B (upper panel). The corresponding external quantum efficiencies (EQE) are plotted in the lower panel.

We used two approaches to determine whether the enhanced V_{oc} for the cascade structure is due to kinetic or thermodynamic effects. In the first, we coat the ITO anode with MoO_3, markedly increasing the anode work function by ca. 2 eV to WF ≈ −6.8 eV.[34] For tetracene-based single donor OPVs with the structure ITO/MoO_3 (100 Å)/Ttn (450 Å)/C_{60} (400 Å)/BCP (100 Å)/Al, analogous to device A, we obtain V_{oc} = 0.53 ± 0.01 V, nearly identical to that on ITO-only anode devices. Likewise, for the device B analogue, we observe V_{oc} = 0.74 ± 0.01 V, again unchanged from the uncoated ITO, device B. Hence, we infer that the difference in V_{oc} between devices A and B arises primarily from the kinetics of molecular electron transfer, rather than from changes in the built-in potential imposed by the Fermi level offset between dissimilar electrodes.

In the second approach, we examined the impact of further shielding the acene π-system at the ITO interface. The orthogonal naphthalene moieties of 5,6-dinaphthyl-tetracene (Dnt) protrude approximately 3.5 Å perpendicular to the plane of its tetracene core. However, the Dnt HOMO energy, ca. −5.37 eV relative to vacuum, is commensurate with those of Dpt and Ttn. Cascade devices consisting of ITO/Dnt (50 Å)/Ttn (350 Å)/Rbn (50 Å)/C_{60} (400 Å)/BCP (100 Å)/Al exhibited inflection points in their *J*−*V* characteristics, resulting in a low fill factor (*FF* = 0.32 ± 0.02), suggesting that the Dnt inhibits charge extraction at the anode. These data reflect the primarily kinetic perturbation induced by shielding the π-system of the material.

The external quantum efficiency for the cascade structure (device B) in Figure 3b is lower than that of device A between λ = 450 and 550 nm. To account for the loss of photocurrent in device B, we performed optical transflectance measurements on organic multilayer stacks identical to those used in both devices but supported on ITO-free glass substrates and uniformly coated with Al (1000 Å). This technique accounts for optical interference and allows the ratio of photons absorbed in the organic layers relative to the number of incident photons to be estimated. Absorption data corresponding to devices A and B are plotted in Figure 3b, showing the largest difference of 20% between λ = 500 and 550 nm. This results from lower absorption coefficients

Table 1. Performance of Cascade and Single-Donor Organic Solar Cell Devices with Structure ITO/Donor/C_{60} 400 Å/BCP 100 Å/Al 1000 Å

device[a]	donor	J_{sc}[b] ± 0.2 mA/cm^2	V_{oc} ± 0.01 V	*FF* ± 0.02	η_p[b] ± 0.1%
A	Ttn	2.9	0.54	0.54	0.83
B	Dpt/Ttn/Rbn	2.6	0.74	0.50	0.95
C	Dpt/Ttn	1.4	0.79	0.37	0.41
ref 9	100 Å Dpt	1.1	0.65	0.41	0.30
ref 7b	200 Å Rbn	2.4	0.92	0.43	0.92
D	Ptn	5.6	0.25	0.40	0.55
E	Ptn/ClAlPc	8.3	0.36	0.46	1.39
ref 30[c]	200 Å ClAlPc	7.4	0.68	0.50	2.10

[a] A, donor = Ttn (450 Å); B = Dpt (50 Å)/Ttn (200 Å)/Rbn (200 Å); C = Dpt (100 Å)/Ttn (350 Å); D = Ptn (600 Å); *E* = Ptn (600 Å)/ClAlPc (300 Å). [b] Under simulated 1 sun illumination, as described in the Experimental Methods. [c] Ag cathode.

dx.doi.org/10.1021/cm200525h |*Chem. Mater.* 2011, 23, 4132–4140

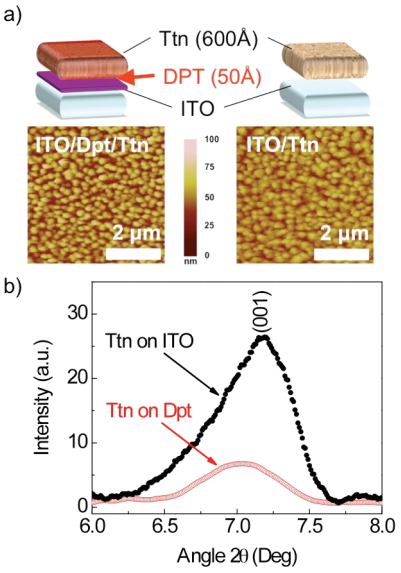

Figure 4. (a) Schematic representation and topographical images obtained by atomic force microscopy for 600 Å thick tetracene (Ttn) films grown on pristine ITO or ITO coated with 50 Å diphenyltetracene (Dpt). (b) Grazing incidence X-ray diffraction (GIXD) peaks for the samples in part a.

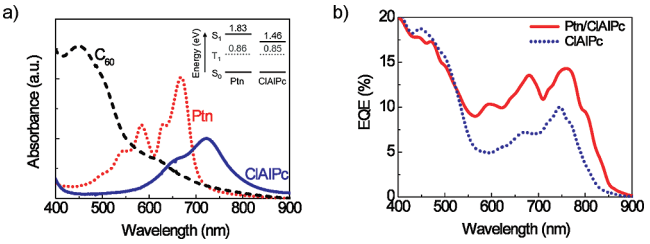

Figure 5. (a) Absorbance spectra for vapor deposited thin films of C_{60} (dashed black trace), pentacene (Ptn, dotted red trace), and chloroaluminum phthalocyanine (ClAlPc, solid blue trace). The inset depicts the lowest singlet and triplet excitonic state energies for Ptn and ClAlPc. (b) External quantum efficiencies illustrating excitation transfer from Ptn to ClAlPc in the cascade device comprising a Ptn (300 Å)/ClAlPc (300 Å) donor layer (solid red trace) compared with a single 300 Å ClAlPc donor layer (dotted blue trace) in ITO/donor/C_{60} (400 Å)/BCP (100 Å)/Al devices.

at λ = 522 nm for Dpt and Rbn, $\alpha = 0.19 \times 10^5$ and 0.55×10^5 cm^{-1}, respectively, while Ttn has $\alpha = 1.20 \times 10^5$ cm^{-1} at the same wavelength. Note that the Dpt and Rbn layers are thinner than the Ttn layer, so the difference in absorbance of the single and multilayer films is not as great as differences in α. Estimating an internal quantum efficiency at λ = 520 nm, according to IQE(λ) = EQE(λ)/$\eta_a(\lambda)$, where $\eta_a(\lambda)$ is the spectral absorbance, one obtains IQE $\approx$ 35% for device A but only 23% for device B. Thus, diminished absorption does not completely account for the photocurrent losses in the latter device.

Because exciton dynamics[8c,22b] and charge mobility[8b,35] depend on morphology, we compared Ttn films grown on Dpt-coated ITO with Ttn films grown directly on ITO. We employed atomic force microscopy and grazing incidence X-ray diffraction (GIXD) to determine surface topography and film morphology. The AFM topographs in Figure 4a for Ttn films grown on ITO and ITO/Dpt exhibit similar submicrometer features, with a root mean square roughness of 9 nm, which is large as a result of film crystallization. The GIXD spectra for ITO/Dpt (50 Å)/Ttn (600 Å) and ITO/Ttn (600 Å) samples in Figure 4b exhibit a Ttn (001) peak at $2\theta = 7.1°$, with full widths at half maxima of 0.62°. Films of Dpt on ITO substrates do not show any discernible X-ray diffraction peaks. However, the intensity in the ITO/Dpt/Ttn spectrum is only 20% of that of the ITO/Ttn sample, implying smaller, misaligned crystalline domains in the ITO/Dpt/Ttn films. Because shorter exciton diffusion lengths are expected for materials disrupted by small domains,[8c] these data suggest that the lower IQE for device B likely stems from reduced exciton diffusion through the Ttn layer.[21a]

An ideal cascade structure should enhance spectral coverage and, thus, J_{sc}, without incurring losses in V_{oc}. The tetracene-based donors used in device B, however, have similar absorption profiles, and thus, to extend spectral coverage, we used cascade structures consisting of a combination of pentacene (Ptn) and aluminum phthalocyanine chloride (ClAlPc) as donors. The principle vibronic progression of Ptn, shown in Figure 5a, is red shifted by ca. 150 nm relative to Ttn. Moreover, Ptn has been shown to possess a high hole mobility.[36] The open circuit voltage for Ptn-based devices is generally low, typically V_{oc} = 0.25 $\pm$ 0.01 V (device structure = ITO/Ptn (600 Å)/C_{60}(400 Å)/BCP/Al). Although its ionization energy, −4.9 eV,[37] should lead to ΔE_{HL} =1.2 eV, the low V_{oc} is likely due to rapid charge recombination at the Ptn/C_{60} heterointerface, possibly a result of the planar structure of Ptn.[7b,11a] As is the situation for Ttn based devices, several groups have published Ptn/C_{60} based OPVs, with efficiencies ranging from 0.55% to 2.1%[38] and V_{oc} as high as 0.35 V. The device parameters reported in Table 1, device E, are comparable to reported values.

Note that ClAlPc forms an energy cascade with Ptn, analogous to the Ttn-based materials series. ClAlPc is transparent between λ = 400 and 600 nm, and its intense low energy Q-band at λ_{max} = 740 nm falls below the Ptn optical absorption edge, as shown in Figure 5a. The S_1 excitonic state for Ptn is 1.83 eV[22b,23b] above the ground state. The singlet excitonic state in ClAlPc is 1.46 eV, calculated from Figure 5a at the wavelength where the absorption onset intensity reaches 15% of that of λ_{max}. Interfacial singlet excitation transfer from Ptn to ClAlPc is exothermic and may proceed via either electron exchange or dipolar interactions at the Ptn/ClAlPc interface. Given that the singlet−triplet splitting is ca. 0.61 eV for ClAlPc[39] and is 0.97 eV for Ptn,[22b] the triplet energies of ClAlPc and Ptn are very close, and triplet excitation transfer from Ptn to ClAlPc is also expected to occur, as the state energy diagram in Figure 5a illustrates. Moreover, the ionization energy for ClAlPc is approximately −5.3 eV,[30,40] which is larger than that of Ptn, allowing for efficient hole transfer from ClAlPc to Ptn. Here, we consider a two-layer cascade donor structure, where the Ptn film is grown directly on ITO in both the single donor (Ptn) and cascade devices. For this comparison, we neglect morphological variation in the Ptn layer in comparing single Ptn donor devices to devices with Ptn/ClAlPc donor layers, because both have Ptn deposited directly on ITO.

Evidence for excitation transfer from Ptn to ClAlPc is apparent by comparing the EQE spectral responses in Figure 5b for a Ptn (300 Å)/ClAlPc (300 Å)-based OPV to those of a device with ClAlPc (300 Å) as the sole donor (ITO/donor/C_{60} (400 Å)/BCP (100 Å)/Al). The EQE response for the Ptn/ClAlPc device has two broad ($\Delta\lambda \sim$ 50 nm) peaks centered near λ = 590 and 675 nm as a result of Ptn absorption and excitation transfer to ClAlPc, with magnitudes of EQE $\sim$ 10 and 15%, respectively.

dx.doi.org/10.1021/cm200525h |*Chem. Mater.* 2011, 23, 4132–4140

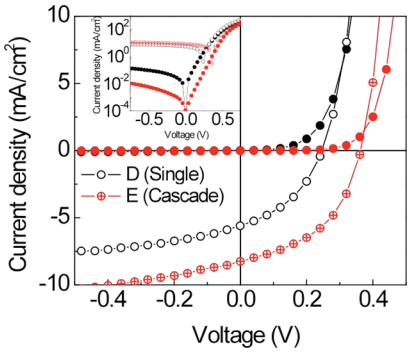

Figure 6. Current voltage characteristics for device E, a Ptn-based cascade donor structure consisting of [Ptn (600 Å)/ClAlPc (300 Å)] (red circle cross) under simulated AM 1.5G 1 sun illumination with spectral mismatch correction to ASTM G173-03,[41] compared with an archetypal [Pentacene (600 Å)] single donor layer (open circle), device D. Complete device structure consists of glass/ITO/donor/C_{60} (400 Å)/BCP (100 Å)/Al (1000 Å). Inset illustrates suppressed dark current (black solid circle) for device E compared on a semilog scale with device D, the Ptn single donor (red solid circle).

The peak at λ = 750 nm and the shoulder near λ = 650 nm correspond to direct optical excitation of ClAlPc. Finally, the broad feature from λ = 400 to 550 nm is primarily due to C_{60} absorption. These data demonstrate that excitation transfer from Ptn to ClAlPc and subsequent charge transfer at ClAlPc/C_{60} leads to efficient photocurrent generation.

The $J-V$ characteristics in the dark and under simulated 1 sun AM 1.5G illumination for a single layer Ptn-based device are shown in Figure 6, along with those obtained for cascade devices comprising a Ptn (600 Å)/ClAlPc (300 Å) donor structure (devices D and E, respectively, in Table 1). For device D, J_{sc} = 5.60 ± 0.23 mA/cm^2, FF = 0.40 ± 0.02, and V_{oc} = 0.25 ± 0.01 V, while for device E there is an increase in voltage to V_{oc} = 0.36 ± 0.01 V. The inset in Figure 6 shows the reduction in the dark current for the cascade device relative to the Ptn-only device (device D); the forward bias dark current at V = 0.25 V is a factor of 30 lower for device E than for device D. The low-energy absorption afforded by the ClAlPc layer enhances the photocurrent obtained from device E (J_{sc} = 8.25 ± 0.23 mA/cm^2) by nearly 50% over that of device D (J_{sc} = 5.60 ± 0.23 mA/cm^2), thus demonstrating the utility of the multidonor exciton transfer system in enhancing photocurrent through broad spectral coverage, while limiting recombination at the D/A interface. Moreover, the hole transport level alignment between the two donor layers ensures slightly exothermic carrier injection from ClAlPc (E_i = −5.3 eV)[30,40] to Ptn (E_i = −4.9 eV).[37] As a result, we observe no decrease in FF for the cascade structure. Indeed, FF = 0.46 ± 0.02 for device E is higher than that for device D, with FF = 0.40 ± 0.02. The enhancements in J_{sc} and V_{oc} lead to an overall power conversion efficiency increase from 0.55% for the Ptn donor device to 1.39% for the cascade structure. A summary of these results and figures of merit for a ClAlPc/C_{60} device from ref 30 is presented in Table 1.

Finally, we note that while the voltage obtained for the Ptn/ClAlPc device (V_{oc} = 0.36 V) is slightly larger than that for the Ptn/C_{60} control device prepared in our laboratory (V_{oc} = 0.25 V), it is significantly lower than the V_{oc} obtained from single-donor ClAlPc/C_{60} devices in the literature (V_{oc} = 0.68 V − 0.84 V).[30,40] This is expected because $\Delta E_{HL} = \varphi_a + \varphi_c + qV_{bi}$, implying that the injection barrier to holes at the anode/donor interface is ∼0.4 eV smaller for Ptn compared to ClAlPc.

SUMMARY

Multiple factors control the efficiencies of organic photovoltaic cells. Balancing the different and often competing materials properties to optimize device performance is often difficult using a single donor or acceptor material. In this work, we demonstrate an approach that partitions performance requirements among several different material layers and interfaces. We found that the efficiency of Ptn/ClAlPc/C_{60} devices can be increased nearly 3-fold over a single donor-layer (Ptn only) OPV cell by increasing the photon absorption through the bilayer absorption, while simultaneously increasing the open circuit voltage based on the reduced recombination at the ClAlPc (vs Ptn)/C_{60} junction.

ASSOCIATED CONTENT

Supporting Information. Absorption coefficient spectra (Dpt, Ttn, and Rbn) and device characteristics for Dnt and MoO_3 based devices. This material is available free of charge via the Internet at http://pubs.acs.org.

AUTHOR INFORMATION

Corresponding Author
*E-mail: mthompso@usc.edu.

ACKNOWLEDGMENT

We acknowledge generous financial support from Global Photonic Energy Corporation, from the Center for Advanced Molecular Photovoltaics (CAMP) (KUS-C1-015-21) of the King Abdullah University of Science and Technology (KAUST). The Center for Energy Nanoscience, an Energy Frontier Research Center funded by the U.S. Department of Energy, Office of Basic Energy Sciences under Award No. DE-SC0001013 is also acknowledged for supporting C.S.W. and R.E.M., who performed the balance of the OPV preparation/testing and analysis presented here. We also acknowledge insightful discussions with Dr. M. Dolores Perez (CNEA) and Professor Chongwu Zhou for the use of his AFM.

REFERENCES

(1) (a) Rand, B. P.; Burk, D. P.; Forrest, S. R. *Phys. Rev. B* **2007**, *75* (11), 115327. (b) Heremans, P.; Cheyns, D.; Rand, B. P. *Acc. Chem. Res.* **2009**, *42* (11), 1740–1747.

(2) (a) Thompson, B. C.; Frechet, J. M. J. *Angew. Chem., Int. Ed.* **2008**, *47* (1), 58–77. (b) Spanggaard, H.; Krebs, F. C. *Sol. Energy Mater. Sol. Cells* **2004**, *83* (2−3), 125–146. (c) Krebs, F. C.; Gevorgyan, S. A.; Gholamkhass, B.; Holdcroft, S.; Schlenker, C.; Thompson, M. E.; Thompson, B. C.; Olson, D.; Ginley, D. S.; Shaheen, S. E.; Alshareef, H. N.; Murphy, J. W.; Youngblood, W. J.; Heston, N. C.; Reynolds, J. R.; Jia, S. J.; Laird, D.; Tuladhar, S. M.; Dane, J. G. A.; Atienzar, P.; Nelson, J.; Kroon, J. M.; Wienk, M. M.; Janssen, R. A. J.; Tvingstedt, K.; Zhang, F. L.; Andersson, M.; Inganas, O.; Lira-Cantu, M.; de Bettignies, R.; Guillerez, S.; Aernouts, T.; Cheyns, D.; Lutsen, L.; Zimmermann, B.; Wurfel, U.; Niggemann, M.; Schleiermacher, H. F.; Liska, P.; Gratzel, M.; Lianos, P.; Katz, E. A.; Lohwasser, W.; Jannon, B. *Sol. Energy Mater. Sol. Cells* **2009**, *93* (11), 1968–1977.

(3) Forrest, S. R. *Nature* **2004**, *428* (6986), 911–918.

(4) (a) Bao, Z.; Dodabalapur, A.; Lovinger, A. J. *Appl. Phys. Lett.* **1996**, *69* (26), 4108–4110. (b) Bao, Z.; Lovinger, A. J.; Dodabalapur, A.

Appl. Phys. Lett. **1996**, *69* (20), 3066–3068. (c) Dimitrakopoulos, C. D.; Malenfant, P. R. L. *Adv. Mater.* **2002**, *14* (2), 99–117.

(5) Roberts, M. E.; Sokolov, A. N.; Bao, Z. N. *J. Mater. Chem.* **2009**, *19* (21), 3351–3363.

(6) (a) Sista, S.; Yao, Y.; Yang, Y.; Tang, M. L.; Bao, Z. A. *Appl. Phys. Lett.* **2007**, *91* (22), 223508. (b) Hong, Z. R.; Lessmann, R.; Maennig, B.; Huang, Q.; Harada, K.; Riede, M.; Leo, K. *J. Appl. Phys.* **2009**, *106* (6), 6. (c) Huang, J. H.; Velusamy, M.; Ho, K. C.; Lin, J. T.; Chu, C. W. *J. Mater. Chem.* **2010**, *20* (14), 2820–2825. (d) Ichikawa, M.; Suto, E.; Jeon, H. G.; Taniguchi, Y. *Org. Electron.* **2010**, *11* (4), 700–704. (e) Kumar, H.; Kumar, P.; Bhardwaj, R.; Sharma, G. D.; Chand, S.; Jain, S. C.; Kumar, V. *J. Phys. D: Appl. Phys.* **2009**, *42* (1), 6. (f) Currie, M. J.; Mapel, J. K.; Heidel, T. D.; Goffri, S.; Baldo, M. A. *Science* **2008**, *321* (5886), 226–228. (g) Zhang, G.; Li, W. L.; Chu, B.; Chen, L. L.; Yan, F.; Zhu, J. Z.; Chen, Y. R.; Lee, C. S. *Appl. Phys. Lett.* **2009**, *94* (14), 143302.

(7) (a) Yang, L. Q.; Zhou, H. X.; You, W. *J. Phys. Chem. C* **2010**, *114* (39), 16793–16800. (b) Perez, M. D.; Borek, C.; Forrest, S. R.; Thompson, M. E. *J. Am. Chem. Soc.* **2009**, *131* (26), 9281–9286.

(8) (a) Coropceanu, V.; Cornil, J.; da Silva, D. A.; Olivier, Y.; Silbey, R.; Bredas, J. L. *Chem. Rev.* **2007**, *107* (4), 926–952. (b) Servet, B.; Horowitz, G.; Ries, S.; Lagorsse, O.; Alnot, P.; Yassar, A.; Deloffre, F.; Srivastava, P.; Hajlaoui, R.; Lang, P.; Garnier, F. *Chem. Mater.* **1994**, *6* (10), 1809–1815. (c) Lunt, R. R.; Benziger, J. B.; Forrest, S. R. *Adv. Mater.* **2010**, *22* (11), 1233.

(9) Barlier, V. S.; Schlenker, C. W.; McAnally, R.; Chin, S. W.; Thompson, M. E. In preparation. 2010.

(10) (a) Shrotriya, V.; Li, G.; Yao, Y.; Moriarty, T.; Emery, K.; Yang, Y. Accurate Measurement and Characterization of Organic Solar Cells *Adv. Funct. Mater.* **2006**, *16* (15), 2016–2023.(b) Emery, K. Measurement and Characterization of Solar Cells and Modules. In *Handbook of Photovoltaic Science and Engineering*; Luque, H. S. A., Ed.; Wiley & Sons: Chichester, U.K., 2003. (c) Matson, R. J.; Emery, K. A.; Bird, R. E. Terrestrial Solar Spectra, Solar Simulation and Solar-Cell Short-Circuit Current Calibration—a Review *Sol. Cells* **1984**, *11* (2), 105–145.

(11) (a) Giebink, N. C.; Lassiter, B. E.; Wiederrecht, G. P.; Wasielewski, M. R.; Forrest, S. R. Ideal Diode Equation for Organic Heterojunctions. II. The Role of Polaron Pair Recombination *Phys. Rev. B* **2010**, *82* (15), 155306–1. (b) Giebink, N. C.; Wiederrecht, G. P.; Wasielewski, M. R.; Forrest, S. R. Ideal Diode Equation for Organic Heterojunctions. I. Derivation and Application *Phys. Rev. B* **2010**, *82* (15), 155305–1.(c) Schlenker, C. W.; Thompson, M. E. The Molecular Nature of Photovoltage Losses in Organic Solar Cells. *Chem. Commun.* **2011**, DOI:10.1039/c0cc04020g.

(12) Moliton, A.; Nunzi, J. M. *Polym. Int.* **2006**, *55* (6), 583–600.

(13) Vandewal, K.; Tvingstedt, K.; Gadisa, A.; Inganas, O.; Manca, J. V. *Phys. Rev. B* **2010**, *81* (12), 125204–1.

(14) Neamen, D. A. *Semiconductor Physics and Devices*, 3rd ed.; McGraw-Hill: New York, 2003.

(15) Maurano, A.; Shuttle, C. C.; Hamilton, R.; Ballantyne, A. M.; Nelson, J.; Zhang, W. M.; Heeney, M.; Durrant, J. R. *J. Phys. Chem. C* **2011**, *115* (13), 5947–5957.

(16) (a) Shuttle, C. G.; Hamilton, R.; O'Regan, B. C.; Nelson, J.; Durrant, J. R. *Proc. Natl. Acad. Sci. USA* **2010**, *107* (38), 16448–16452. (b) Shuttle, C. G.; Hamilton, R.; Nelson, J.; O'Regan, B. C.; Durrant, J. R. *Adv. Funct. Mater.* **2010**, *20* (5), 698–702. (c) Maurano, A.; Hamilton, R.; Shuttle, C. G.; Ballantyne, A. M.; Nelson, J.; O'Regan, B.; Zhang, W. M.; McCulloch, I.; Azimi, H.; Morana, M.; Brabec, C. J.; Durrant, J. R. *Adv. Mater.* **2010**, *22* (44), 4987–4992. (d) Hamilton, R.; Shuttle, C. G.; O'Regan, B.; Hammant, T. C.; Nelson, J.; Durrant, J. R. *J. Phys. Chem. Lett.* **2010**, *1* (9), 1432–1436. (e) Shuttle, C. G.; O'Regan, B.; Ballantyne, A. M.; Nelson, J.; Bradley, D. D. C.; Durrant, J. R. *Phys. Rev. B* **2008**, *78* (11), 113201. (f) Shuttle, C. G.; O'Regan, B.; Ballantyne, A. M.; Nelson, J.; Bradley, D. D. C.; de Mello, J.; Durrant, J. R. *Appl. Phys. Lett.* **2008**, *92* (9), 093311. (g) Shuttle, C. G.; Maurano, A.; Hamilton, R.; O'Regan, B.; de Mello, J. C.; Durrant, J. R. *Appl. Phys. Lett.* **2008**, *93* (18), 183501. (h) Heutz, S.; Nogueira, A. F.; Durrant, J. R.; Jones, T. S. *J. Phys. Chem. B* **2005**, *109* (23), 11693–11696.

(17) Erwin, P.; Thompson, M. E. *Appl. Phys. Lett.* **2011**, *98* (22), 223305.

(18) (a) Jenekhe, S. A.; Osaheni, J. A. *Science* **1994**, *265* (5173), 765–768. (b) Tvingstedt, K.; Vandewal, K.; Gadisa, A.; Zhang, F. L.; Manca, J.; Inganas, O. *J. Am. Chem. Soc.* **2009**, *131* (33), 11819–11824.

(19) Beljonne, D.; Cornil, J.; Muccioli, L.; Zannoni, C.; Bredas, J. L.; Castet, F. *Chem. Mater.* **2011**, *23* (3), 591–609.

(20) (a) Sato, N.; Inokuchi, H.; Silinsh, E. A. Reevaluation of Electronic Polarization Energies in Organic Molecular-Crystals *Chem. Phys.* **1987**, *115* (2), 269–277.(b) Silinsh, E. A.; Čápek, V. *Organic Molecular Crystals*; American Institute of Physics: New York, 1994. (c) Sato, N.; Seki, K.; Inokuchi, H. Polarization Energies of Organic-Solids Determined by Ultraviolet Photoelectron-Spectroscopy *J. Chem. Soc., Faraday Trans.* **1981**, *77*, 1621–1633.

(21) (a) Shao, Y.; Sista, S.; Chu, C. W.; Sievers, D.; Yang, Y. *Appl. Phys. Lett.* **2007**, *90* (10), 103501. (b) Burdett, J. J.; Muller, A. M.; Gosztol, D.; Bardeen, C. J. *J. Chem. Phys.* **2010**, *133* (14), 12. (c) Cicoira, F.; Santato, C.; Dinelli, F.; Murgia, M.; Loi, M. A.; Biscarini, F.; Zamboni, R.; Heremans, P.; Muccini, M. *Adv. Funct. Mater.* **2005**, *15* (3), 375–380.

(22) (a) Swenberg, C. E.; Stacy, W. T. *Chem. Phys. Lett.* **1968**, *2*, 327–328. (b) Thorsmolle, V. K.; Averitt, R. D.; Demsar, J.; Smith, D. L.; Tretiak, S.; Martin, R. L.; Chi, X.; Crone, B. K.; Ramirez, A. P.; Taylor, A. J. *Phys. Rev. Lett.* **2009**, *102* (1), 017401. (c) Burdett, J. J.; Muller, A. M.; Gosztol, D.; Bardeen, C. J. *J. Chem. Phys.* **2010**, *133* (14), 144506. (d) Grumstrup, E. M.; Johnson, J. C.; Damrauer, N. H. *Phys. Rev. Lett.* **2010**, *105*, 25.

(23) (a) Lee, J.; Jadhav, P.; Baldo, M. A. *Appl. Phys. Lett.* **2009**, *95* (3), 033301. (b) Rao, A.; Wilson, M. W. B.; Hodgkiss, J. M.; Albert-Seifried, S.; Bassler, H.; Friend, R. H. *J. Am. Chem. Soc.* **2010**, *132* (36), 12698–12703.

(24) Jadhav, P. J.; Mohanty, A.; Sussman, J.; Lee, J.; Baldo, M. A. *Nano Lett.* **2011**, *11* (4), 1495–1498.

(25) Liu, D. K. K.; Faulkner, L. R. *J. Am. Chem. Soc.* **1977**, *99* (14), 4594–4599.

(26) (a) Ding, H. J.; Gao, Y. L. *Appl. Phys. A: Mater. Sci. Process.* **2009**, *95* (1), 89–94. (b) Wang, L.; Chen, S.; Liu, L.; Qi, D. C.; Gao, X. Y.; Wee, A. T. S. *Appl. Phys. Lett.* **2007**, *90* (13), 132121. (c) Nakayama, Y.; Machida, S.; Minari, T.; Tsukagishi, K.; Noguchi, Y.; Ishii, H. *Appl. Phys. Lett.* **2008**, *93* (17), 173305.

(27) (a) Pope, M. *Trans. N.Y. Acad. Sci.* **1966**, *29* (1), 53. (b) Pope, M.; Burgos, J.; Giachino, J. *J. Chem. Phys.* **1965**, *43* (9), 3367. (c) Hirooka, T.; Tanaka, K.; Kuchitsu, K.; Fujihira, M.; Inokuchi, H.; Harada, Y. *Chem. Phys. Lett.* **1973**, *18* (3), 390–393. (d) Seki, K.; Inokuchi, H.; Harada, Y. *Chem. Phys. Lett.* **1973**, *20* (2), 197–200.

(28) Roberts, S. T.; Schlenker, C. W.; Barlier, V. S.; McAnally, R. E.; Zhang, Y.; Mastron, J. N.; Thompson, M. E.; Bradforth, S. E. *J. Phys. Chem. Lett.* **2011**, *2* (2), 48–54.

(29) Chu, C. W.; Shao, Y.; Shrotriya, V.; Yang, Y. *Appl. Phys. Lett.* **2005**, *86* (24), 243506.

(30) Bailey-Salzman, R. F.; Rand, B. P.; Forrest, S. R. *Appl. Phys. Lett.* **2007**, *91* (1), 013508.

(31) Burgdorff, C.; Kircher, T.; Lohmannsroben, H. G. *Spectrochim. Acta, Part A* **1988**, *44* (11), 1137–1141.

(32) (a) D'Andrade, B. W.; Datta, S.; Forrest, S. R.; Djurovich, P.; Polikarpov, E.; Thompson, M. E. *Org. Electron.* **2005**, *6* (1), 11–20. (b) Djurovich, P. I.; Mayo, E. I.; Forrest, S. R.; Thompson, M. E. *Org. Electron.* **2009**, *10* (3), 515–520.

(33) Frank, K. H.; Yannoulis, P.; Dudde, R.; Koch, E. E. *J. Chem. Phys.* **1988**, *89* (12), 7569–7576.

(34) (a) Tokarz-Sobieraj, R.; Hermann, K.; Witko, M.; Blume, A.; Mestl, G.; Schlogl, R. *Surf. Sci.* **2001**, *489* (1−3), 107–125. (b) Irfan; Ding, H. J.; Gao, Y. L.; Kim, D. Y.; Subbiah, J.; So, F. *Appl. Phys. Lett.* **2010**, *96* (7), 73304. (c) Kroger, M.; Hamwi, S.; Meyer, J.; Riedl, T.; Kowalsky, W.; Kahn, A. *Appl. Phys. Lett.* **2009**, *95* (12), 123301.

(35) McCulloch, I.; Heeney, M.; Bailey, C.; Genevicius, K.; Macdonald, I.; Shkunov, M.; Sparrowe, D.; Tierney, S.; Wagner, R.; Zhang, W. M.; Chabinyc, M. L.; Kline, R. J.; McGehee, M. D.; Toney, M. F. *Nat. Mater.* **2006**, *5* (4), 328–333.

(36) Nelson, S. F.; Lin, Y. Y.; Gundlach, D. J.; Jackson, T. N. *Appl. Phys. Lett.* **1998**, *72* (15), 1854–1856.
(37) (a) Armstrong, N. R.; Wang, W. N.; Alloway, D. M.; Placencia, D.; Ratcliff, E.; Brumbach, M. *Macromol. Rapid Commun.* **2009**, *30* (9−10), 717–731. (b) Kahn, A.; Koch, N.; Gao, W. Y. *J. Polym. Sci., Part B: Polym. Phys.* **2003**, *41* (21), 2529–2548.
(38) (a) Potscavage, W. J.; Yoo, S.; Kippelen, B. *Appl. Phys. Lett.* **2008**, *93* (19), 193308. (b) Cheyns, D.; Gommans, H.; Odijk, M.; Poortmans, J.; Heremans, P. *Sol. Energy Mater. Sol. Cells* **2007**, *91* (5), 399–404. (c) Palilis, L. C.; Lane, P. A.; Kushto, G. P.; Purushothaman, B.; Anthony, J. E.; Kafafi, Z. H. *Org. Electron.* **2008**, *9* (5), 747–752.
(39) Darwent, J. R.; Douglas, P.; Harriman, A.; Porter, G.; Richoux, M. C. *Coord. Chem. Rev.* **1982**, *44* (1), 83–126.
(40) Kim, D. Y.; So, F.; Gao, Y. L. *Sol. Energy Mater. Sol. Cells* **2009**, *93* (9), 1688–1691.
(41) ASTM G173. *ASTM G173-03(2008) Standard Tables for Reference Solar Spectral Irradiances: Direct Normal and Hemispherical on 37° Tilted Surface*; ASTM International: West Conshohocken, PA, 2008.